

Clustering of finite-size particles in turbulence

L. Fiabane,^{1,*} R. Zimmermann,¹ R. Volk,¹ J.-F. Pinton,¹ and M. Bourgoin²

¹*Laboratoire de Physique, ENS de Lyon, UMR CNRS 5672, Université de Lyon, France*

²*LEGI, UMR CNRS 5519, Université Joseph Fourier, Grenoble, France*

(Received 24 May 2012; published 21 September 2012)

We investigate experimentally the spatial distributions of heavy and neutrally buoyant particles of finite size in a fully turbulent flow. Because their Stokes number (i.e., the ratio of the particle viscous relaxation time to a typical flow time scale) is close to unity, one may expect both classes of particles to aggregate in specific flow regions. This is not observed. Using a Voronoï analysis we show that neutrally buoyant particles sample turbulence homogeneously, whereas heavy particles do cluster. These results show that several dimensionless numbers are needed in the modeling (and understanding) of the behavior of particles entrained by turbulent motions.

DOI: [10.1103/PhysRevE.86.035301](https://doi.org/10.1103/PhysRevE.86.035301)

PACS number(s): 47.27.Gs, 47.27.T–, 82.70.–y

Turbulent flows laden with particles are widely found in industry and nature; their study is therefore of great interest and holds many fundamental aspects, issues, and limits still to be explored. One striking feature of these flows is the trend for the particles to concentrate in specific regions of the carrier flow. This has been observed and investigated for a long time both in experiments and simulations, and it is still widely studied (see the review paper [1] and references therein). The focus is usually put on small (namely, much smaller than the dissipation scale η of the flow) and heavy particles (with a high density compared to that of the fluid), especially in numerical studies. Because of their high specific density, the dynamics of such small and heavy inertial particles deviates from that of the carrier flow. Clustering phenomena are then one of the many manifestations of these inertial effects, generally attributed to the centrifugal expulsion of heavy particles from turbulent vortices, and more recently to a sticking effect of zero-acceleration points of the carrier flow [2]. Other studies indicate that light particles exhibit the same trend to cluster but with different cluster geometries [3,4]. Finally, tracers (which ought to be neutrally buoyant and much smaller than η) are used as seeds to characterize the flow dynamics and should not cluster. As small and heavy particles, finite-size heavy particles have been found to cluster [5]. However, the case of finite-size neutrally buoyant particles (with a diameter significantly larger than η) has never been treated to our knowledge in the context of preferential concentration. Such particles are known experimentally [6–8] and numerically [9,10] to differ from tracers, with in particular different acceleration statistics. But existing studies have focused on the dynamics of isolated particles, not on the spatial structuration of laden flows. Whether they cluster or not remains an open question.

Particles interacting with a turbulent flow are commonly characterized by their Stokes number, that is, the ratio between the particle viscous relaxation time τ_p and a typical time scale of the flow. Dealing with finite-size particles, we use the same definition as in Refs. [11,12], using the eddy-turnover time at the scale of the particle, τ_d , as the time scale of the flow, and a corrective factor f_ϕ based on the Reynolds number at particle

scale: $St \equiv \tau_p/\tau_d = f_\phi \phi^{4/3} (1 + 2\Gamma)/36$, where $\Gamma = \rho_p/\rho_f$ is the particle to fluid density ratio and $\phi = d/\eta$ is the particle diameter normalized by the dissipation scale (note that our conclusions remain the same using a point-particle definition of the Stokes number). This dimensionless number is often used as the key parameter to characterizing particle dynamics in turbulence, using simple Stokesian models where the dominant force acting on the particle is taken as the drag due to the difference between the particle velocity and that of the fluid. These models predict preferential concentration of particles with nonvanishing Stokes number, with a maximal segregation for St around unity [13,14]. This behavior is confirmed, at least qualitatively, in experiments with small and heavy particles [15]. In the present study we address the case of finite-size particles (both neutrally buoyant and heavier than the fluid) and investigate the particle concentration field as a function of their Stokes number in a homogeneous and isotropic turbulent flow. First, we describe the experimental setup and the data processing used. Then, we describe the results on spatial structuration for finite-size particles. We finish with a brief discussion and conclusions.

To study the behaviors of both neutrally buoyant and heavy particles, we use water as the carrier fluid. The turbulence is generated in the Lagrangian Exploration Module (LEM, see Fig. 1), whose characteristics are described in detail in Ref. [16] and summed up in Table I. The LEM produces turbulence in a closed water flow forced by 12 impellers evenly distributed on the faces of an icosahedral vessel. Here, all impellers rotate simultaneously at the same constant frequency f_{imp} which can be varied from 2 Hz up to 12 Hz; opposing impellers form counterrotating pairs. This produces a very homogeneous and isotropic turbulence in a significant central region of the device of the order of $(15 \text{ cm})^3$, with the integral length of the order of 5 cm [16]. It also permits us to obtain high Reynolds number turbulent flow with mean velocities much weaker than the fluctuations near the center of the apparatus. Acquisitions are performed using 8-bit digital imaging at a resolution corresponding to a visualization window of the order of $16 \times 12 \text{ cm}$ in the center of the LEM. The visualization zone is illuminated by a 100 W Nd:YAG pulsed laser synchronized with the camera, creating a green light sheet with millimetric thickness. The camera is equipped with a macro lens. A

*lionel.fiabane@ens-lyon.org

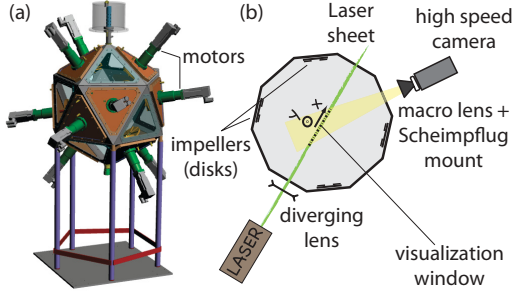


FIG. 1. (Color online) (a) CAD drawing of the LEM. (b) Schematic upper view of the setup.

Scheimpflug mount compensates for the depth of field effects resulting from the angle between the camera and the laser sheet (see Fig. 1). Images are recorded at a low repetition rate of 2.5 Hz sufficient to address particle spatial distribution as we ensemble average over 2000 independent flow realizations for each experiment (particle dynamics is not addressed here).

We explore the behavior of two kinds of finite-size particles: neutrally buoyant and heavy ones. Regarding the neutrally buoyant particles, we use expanded polystyrene particles whose density has been irreversibly adjusted (prior to actual experiments) by moderate heating so that the density ratio to water is $1 \leq \Gamma_n \leq 1.015$. Depending on their size, the particles can be regarded as *tracers* following the carrier flow dynamics, or as *finite-size particles* whose dynamics departs from that of the flow. The limit for tracer behavior is known to be $d_n \simeq 5\eta$, whereas finite-size effects appear for $d_n > 5\eta$ [7,8,17]. In our case the particle diameter is $d_n = 700 \pm 20 \mu\text{m}$ and ranges from 4.5η to 17η (from the lowest to the highest investigated R_λ). Hence, our particles transit from tracers to finite-size particles as f_{imp} increases. As for heavy particles, we use slightly polydispersed sieved glass particles with diameters $225 \pm 25 \mu\text{m}$ and a density ratio $\Gamma_h = 2.5$, making them *inertial particles*. The neutrally buoyant particles cover a Stokes number from 0.38 to 1.23, while the heavy particles cover a Stokes number from 0.25 to 1.04 (see Table I). These two ranges overlap allowing some comparison. Since for each class of particles the diameter and density are kept constant, the Stokes number is varied by tuning the flow dissipation time scale. Therefore, it cannot be varied independently of the Reynolds number of the carrier flow.

We identify the particles on the images as local maxima with light intensity higher than a threshold, assuming in a first approximation that all the particles illuminated in the laser sheet belong to one plane. The center of the particles is determined as the center of mass of all the pixels surrounding one local maximum. Due to the high contrast between the light diffused by the particles and the background, changing slightly the threshold value does not significantly impact the number of detected particles, which is of order 100 (150) for the neutrally buoyant (heavy) particles (note that dealing with finite-size particles, the maximum authorized seeding density is drastically reduced by particles in the bulk blocking or eclipsing the image of particles in the laser sheet, compared to, e.g., experiments with small particles where thousands of particles per image are typically recorded [15]). The number of detected neutrally buoyant particles remains constant in time, indicating a good stationarity of seeding concentration as expected for nonsettling particles. However large heavy particles tend to settle for low impeller rotation rates f_{imp} . The heavy particles we consider here are sufficiently large to be considered as *finite size* and sufficiently small to prevent significant settling, since the entrainment by the flow is still capable of keeping them in suspension. Because of this limitation we did not consider bigger particles, and we did not investigate regimes where $f_{\text{imp}} < 2 \text{ Hz}$ (for which settling becomes important). Moreover, we make sure that the flow is already set in motion when the particles are inserted in the vessel to prevent them from settling immediately. Additionally, the number of particles per image is monitored, and experiments are repeated (after reloading particles) if too many are found to have settled (a typical experiment can run a few hours with relatively stationary seeding conditions).

The particle concentration field is investigated using Voronoï diagrams; this technique recently introduced for the investigation of preferential concentration of small water droplets in a turbulent airflow [15] was shown to be particularly efficient and robust to diagnose and quantify clustering phenomena. A given raw image, the detected particles, and the associated Voronoï diagram are provided for neutrally buoyant particles in Figs. 2(a) and 2(b); Fig. 2(c) shows a typical Voronoï diagram for the heavy particle case. The Voronoï diagrams give a tessellation of a two-dimensional space where each cell of the tessellation is linked to a detected particle, with all points of one cell closer to its associated particle than to any other particle. Thus, the area of each Voronoï cell is the inverse

TABLE I. Turbulence characteristics. f_{imp} : rotation frequency of the 12 impellers; u' : fluctuation velocity of the flow; ε : energy dissipation rate; $\eta \equiv (\nu^3/\varepsilon)^{1/4}$ and $\tau_\eta \equiv (\nu/\varepsilon)^{1/2}$: Kolmogorov length and time scales of the flow; $R_\lambda \equiv (15u'^4/\nu\varepsilon)^{-1/2}$: Taylor microscale Reynolds number; St_n and St_h : Stokes numbers of neutrally buoyant and heavy particles, respectively.

f_{imp} (Hz)	u' (cm/s)	ε (m^2/s^3)	η (μm)	τ_η (ms)	R_λ	St_n	St_h
2	4	0.0016	159	24.9	160	0.38 ± 0.02	0.25 ± 0.04
4	8	0.0144	92	8.3	210	0.64 ± 0.03	0.46 ± 0.09
6	12	0.0611	64	4.0	260	0.87 ± 0.04	0.68 ± 0.11
8	17	0.1086	55	3.0	310	0.98 ± 0.04	0.78 ± 0.11
10	22	0.2087	47	2.2	360	1.11 ± 0.05	0.92 ± 0.11
12	26	0.3518	41	1.7	395	1.23 ± 0.05	1.04 ± 0.16

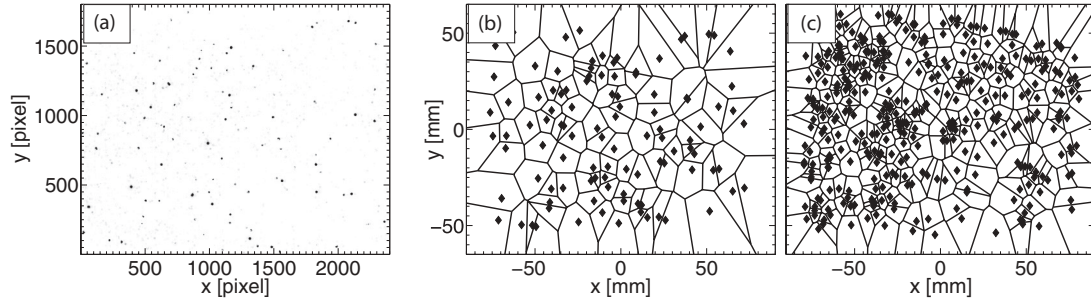


FIG. 2. (a) Typical raw acquired image of neutrally buoyant particles and (b) the detected particles located in real space with the associated Voronoi diagram. (c) Heavy particles located in real space with the associated Voronoi diagram (corresponding raw image not shown).

of the local concentration of particles, i.e., Voronoi area fields are a measure of the local concentration fields at interparticle length scale. To compare the results of experiments made with different amounts of detected particles per image, the Voronoi area is normalized using the average Voronoi area \bar{A} defined as the mean particles concentration inverse, independent of the spatial organization of the particles. Therefore, we focus in the rest of this Rapid Communication on the distribution of the normalized Voronoi area $\mathcal{V} \equiv A/\bar{A}$. Clustering properties are quantified by comparing the probability density function (PDF) of Voronoi cell areas obtained from the experiments to that of a synthetic random Poisson process (RPP) whose shape is well approximated by a Gamma distribution [18].

The PDFs of Voronoi cell areas for the different experiments described in Table I are plotted in Fig. 3, as well as the Gamma distribution approximation for a RPP. In the case of neutrally buoyant particles, all PDFs collapse and no Stokes number dependency is found. An important finding of the present work is that these PDFs are almost indistinguishable from the RPP distribution, meaning large neutrally buoyant particles do not exhibit any preferential concentration whatever their Stokes number. In the case of heavy particles, the PDFs clearly depart from the RPP distribution, with higher probability of finding depleted regions (large Voronoi areas) and concentrated regions (small Voronoi areas), which is the signature of preferential concentration. Furthermore, the shape of the PDF clearly depends on experimental parameters (St_h and/or R_λ). Interestingly, this dependence is stronger for the small Voronoi area tails, whereas the tail for large Voronoi areas (corresponding to depleted regions) appears to be more robust. This was also observed for small inertial particles [15,19]. The level of clustering can be further quantified using the standard deviation of the normalized Voronoi areas $\sigma_V = \sqrt{\langle \mathcal{V}^2 \rangle - 1}$, plotted in Fig. 4. For neutrally buoyant particles we find a constant value $\sigma_V \simeq 0.53$, which is the expected value for a RPP. For heavy particles we find $\sigma_V > 0.53$ for all the experimental configurations investigated, revealing the presence of clustering. This result is in agreement with previous measurements [5] that find clustering for large ($\phi \simeq 4$) and heavy ($\Gamma = 1.4$) particles. We find the clustering level to globally decrease as St_h and/or R_λ increase, with no hint of

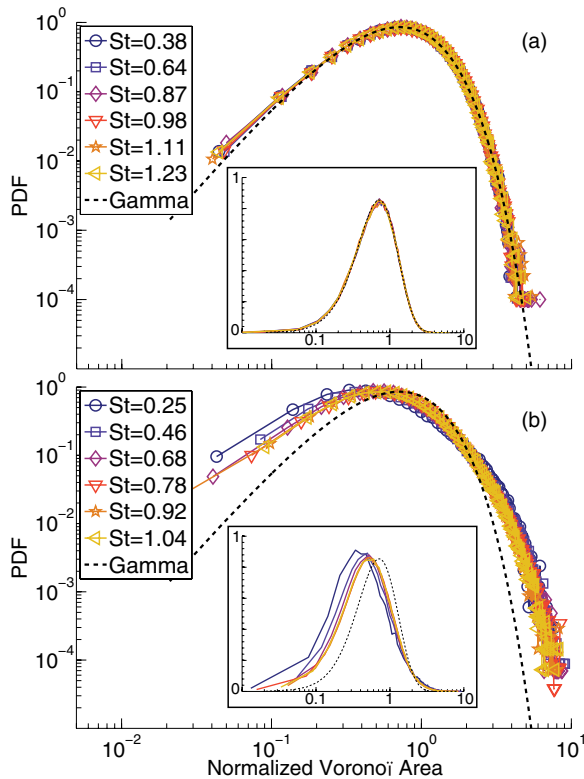


FIG. 3. (Color online) Superposition of the normalized Voronoi area PDFs for six experiments with varying Stokes number (plain lines) and a Gamma distribution (dashed line). Inserts represent the same results with linear ordinates. (a) Neutrally buoyant particles. (b) Heavy particles.

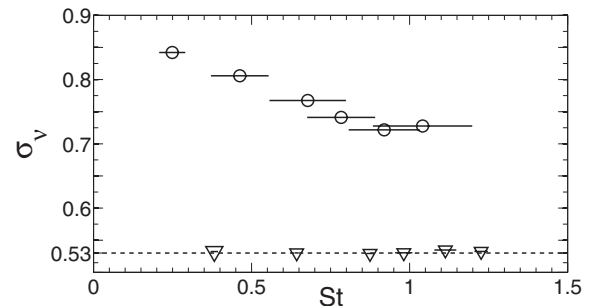


FIG. 4. Standard deviations of the normalized Voronoi areas vs the Stokes number with error bars (plain lines) for neutrally buoyant (∇) and heavy particles (\circ), to compare with $\sigma_V^{\text{RPP}} \simeq 0.53$ in the case of a RPP.

maximum clustering for St_h around unity. This is contrary to common observations: for numerical Stokesian models [13,14] a maximum is found for $St \simeq 0.6$; for experiments with small particles [15,19], a peak is observed for $St \gtrsim 1$ while Ref. [20] found a mild maximum for $St \simeq 1$. If a maximum of clustering exists in our case (which is reasonable assuming that tracer behavior is to be recovered for $St_h \rightarrow 0$), the peak would be at $St_h < 0.25$. However, the limit $St_h \rightarrow 0$ (i.e., $R_\lambda \rightarrow 0$) could not be explored here due to the settling effects at low R_λ . The clustering properties (Stokes number dependence and clusters geometry) for such finite-size and heavy particles go beyond the scope of the present research and will be investigated in future experiments.

Two important conclusions can be drawn from these results. (i) While inertial Stokesian models predict clustering within the explored range of St , this is not observed in the specific case of finite-size neutrally buoyant particles. Consequently, even though they do not behave as tracers, such particles are clearly not of the *inertial* class. The absence of clustering also supports experimental results on the dynamics of finite-size neutrally buoyant particles [7,8,17] suggesting that simple time-response effects are not sufficient to describe the particle-flow interaction and that other mechanisms (such as the role

of pressure increments at the scale of the particle) are to be accounted for. (ii) Subsequently, the Stokes number by itself cannot be taken as sufficient to characterize clustering, because we have shown that particles with similar Stokes numbers may or not exhibit preferential concentration. Note that the limitation of the Stokes number has previously been shown for dynamical properties (rather than spatial distribution properties as illustrated here) of both isolated particles in turbulent flows [3,21] and two-way coupling effects [22]. These observations combined with ours stimulate the need for further investigations on the possible connection between dynamical features and preferential sampling of particles (including for instance turbophoresis and stick-sweep mechanisms [2], but also ergodic mechanisms [23]), by coupling Voronoï analysis of particles distribution to Lagrangian tracking [4,15].

We are currently investigating which set of parameters $f(\phi, \Gamma, R_\lambda, \dots)$ drives the finite-size particle clustering, in particular by exploring how clustering is affected when Stokes number is varied (using particles with different sizes) at a fixed Reynolds number.

This work is partially supported by the ANR project TEC. We thank D. Le Tourneau for the manufacturing of the LEM.

-
- [1] R. Monchaux, M. Bourgoïn, and A. Cartellier, *Int. J. Multiphase Flow* **40**, 1 (2012).
 - [2] S. Goto and J. C. Vassilicos, *Phys. Rev. Lett.* **100**, 054503 (2008).
 - [3] E. Calzavarini, M. Kerscher, D. Lohse, and F. Toschi, *J. Fluid Mech.* **607**, 13 (2008).
 - [4] Y. Tagawa, J. M. Mercado, V. N. Prakash, E. Calzavarini, C. Sun, and D. Lohse, *J. Fluid Mech.* **693**, 201 (2012).
 - [5] M. Guala, A. Liberzon, K. Hoyer, A. Tsinober, and W. Kinzelbach, *J. Turb.* **9**, N34 (2008).
 - [6] G. A. Voth, A. La Porta, A. M. Crawford, J. Alexander, and E. Bodenschatz, *J. Fluid Mech.* **469**, 121 (2002).
 - [7] N. M. Qureshi, M. Bourgoïn, C. Baudet, A. Cartellier, and Y. Gagne, *Phys. Rev. Lett.* **99**, 184502 (2007).
 - [8] R. D. Brown, Z. Warhaft, and G. A. Voth, *Phys. Rev. Lett.* **103**, 194501 (2009).
 - [9] E. Calzavarini, R. Volk, M. Bourgoïn, E. L ev eque, J.-F. Pinton, and F. Toschi, *J. Fluid Mech.* **630**, 179 (2009).
 - [10] H. Homann and J. Bec, *J. Fluid Mech.* **651**, 81 (2010).
 - [11] F. G. Schmitt and L. Seuront, *J. Marine Systems* **70**, 263 (2008).
 - [12] H. Xu and E. Bodenschatz, *Phys. D* **237**, 2095 (2008).
 - [13] J. Bec, L. Biferale, M. Cencini, A. Lanotte, S. Musacchio, and F. Toschi, *Phys. Rev. Lett.* **98**, 084502 (2007).
 - [14] S. W. Coleman and J. C. Vassilicos, *Phys. Fluids* **21**, 113301 (2009).
 - [15] R. Monchaux, M. Bourgoïn, and A. Cartellier, *Phys. Fluids* **22**, 103304 (2010).
 - [16] R. Zimmermann, H. Xu, Y. Gasteuil, M. Bourgoïn, R. Volk, J.-F. Pinton, and E. Bodenschatz, *Rev. Sci. Instrum.* **81**, 055112 (2010).
 - [17] R. Volk, E. Calzavarini, E. L ev eque, and J.-F. Pinton, *J. Fluid Mech.* **668**, 223 (2011).
 - [18] J.-S. Ferenc and Z. N eda, *Physica A* **385**, 518 (2007).
 - [19] M. Obligado, M. Missaoui, R. Monchaux, A. Cartellier, and M. Bourgoïn, *J. Phys.: Conf. Ser.* **318**, 052015 (2011).
 - [20] J. R. Fessler, J. D. Kulick, and J. K. Eaton, *Phys. Fluids* **6**, 3742 (1994).
 - [21] N. M. Qureshi, U. Arrieta, C. Baudet, A. Cartellier, Y. Gagne, and M. Bourgoïn, *Eur. Phys. J. B* **66**, 531 (2008).
 - [22] F. Lucci, A. Ferrante, and S. Elghobashi, *Phys. Fluids* **23**, 025101 (2011).
 - [23] K. Gustavsson and B. Mehlig, *Europhys. Lett.* **96**, 60012 (2011).